Simulation of monsoon intraseasonal oscillations in a coarse resolution aquaplanet GCM

R. S. Ajayamohan,[1] Boualem Khouider[2] and Andrew J. Majda[1,3]

[1]Center for Prototype Climate Modelling,

New York University, Abu Dhabi, UAE.

Email: Ajaya.Mohan@nyu.edu

[2]Department of Mathematics and

Statistics, University of Victoria, BC,

Canada.

[3]Department of Mathematics & Center

for Atmosphere and Ocean Sciences,

Courant Institute of Mathematical Sciences,

New York University, NY, USA

The skill of the global climate models (GCMs) to realistically simulate the Monsoon Intraseasonal Oscillations (MISOs) is hindered by the inadequacy of their cumulus parameterization schemes. Here, we show that by coupling a simple multicloud parameterization to an aquaplanet GCM at coarse resolution, realistic MISOs can be simulated. We conduct three different simulations with a fixed but non-homogeneous SST mimicking the Indian Ocean/Western Pacific warm pool centered at the three latitudes 5°N, 10°N and 15°N, respectively, to replicate the seasonal migration of the Tropical Convergence Zone (TCZ). This results in the generation of mean circulation resembling the monsoonal flow pattern in boreal summer. Succession of eastward propagating Madden-Julian Oscillation (MJO) disturbances with phase speeds, amplitude and physical structure similar to summer MJOs are simulated when the WP is at 5°N. When the WP is located over 10°N, northward and eastward propagating MISOs are simulated. This case captures the meridional see-saw of convection between the continental and oceanic TCZ observed during boreal summer over the south Asian continents. Westward propagating Rossby-wave like disturbances are simulated when the WP is moved over 15°N congruous with the synoptic disturbances seen over the monsoon trough region. The initiation mechanism of intraseasonal oscillations in the the model is believed to be a combination of intermittent organized convective events interacting with the large scale circulation and internal dynamics.

1. Introduction

The dry and wet seasons over the tropics typically fluctuate between 10 and 90 days, referred to as tropical intraseasonal variability [*Lau and Waliser*, 2012]. The eastward propagating Madden-Julian Oscillations [MJO; *Madden and Julian*, 1971] and northward propagating monsoon intraseasonal oscillations [MISO; *Goswami*, 2012] are the dominant components of the intraseasonal variability in the tropical atmosphere. These large-scale planetary scale oscillations are visible in atmospheric winds and precipitation with coherent signals in many other variables. The MJO waves originate over the warm waters of the Indian Ocean (IO) and propagate eastward towards the maritime continent and Pacific Ocean with a speed of $\approx 5\text{ms}^{-1}$ and are very strong in boreal winter. In boreal summer, the MISO originates over the IO and moves northeastward with a speed of $\approx 2\text{ms}^{-1}$, in tune with the movement of the tropical convergence zone causing heavy rainfall over the south-Asian continents [*Gadgil*, 2003]. The tropical intraseasonal oscillations interacts with the underlying oceans and influences the global weather and climate system [*Zhang*, 2005].

In spite of recent intensive research efforts [*Zhang*, 2005; *Lau and Waliser*, 2012], accurately simulating and predicting the intraseasonal oscillations using state-of-the-art GCMs remains challenging. Several missing links in understanding the physics and dynamics of the MJO/MISO have motivated co-ordinated efforts in observational and diagnostic studies in the last few years [*Zhang et al.*, 2013; *Bhat et al.*, 2001; *Rao*, 2005]. Realistic simulation of the observed phase and amplitude of the MJO/MISO is the most common bias seen in the climate model simulations. When eastward propagating MJOs are simulated, they are either too weak, or their spatial distributions and seasonal cycles are unrealistic [*Lin et al.*, 2006; *Kim et al.*, 2009]. Similar issues exist in the simulation of MISO as well [*Sperber et al.*, 2013]. It is also noted that marked improvements have been made by a few GCMs in simulating realistic MJO/MISO [*Crueger et al.*, 2013].

Here, we use an aquaplanet model with a prescribed warm pool to simulate MISOs. This model is designed without land or topography, without ocean-atmospheric coupling and without moist extratropical dynamics. A mask restricting heating and cooling to the tropical belt is applied over 30°S-30°N or 40°S-40°N [see below; *Khouider et al.*, 2011]. Here, we show that with an appropriate warm pool in the location of the Tropical Convergence Zone (TCZ), a realistic simulation of MISO can be achieved. The main element is the use of a simple-prototype multicloud model parameterization that is designed to capture the observed cloud morphology and dynamics of organized convection [*Khouider and Majda*, 2006a; *Khouider et al.*, 2011]. The multicloud parameterization scheme is built on the observed paradigm of organized cloud structure observed for both MJO and MISO [*Johnson et al.*, 1999; *Mapes et al.*, 2006; *Abhik et al.*, 2013] using three cloud types, congestus, deep, and stratiform. This methodology is in contrast with the traditional plume-based and large-scale forcing type parameterizations. The multicloud cloud model represents the unresolved mesoscale dynamics associated with organized convection by capturing the transition from shallow to deep convection through the progressive moistening due to congestus activity [*Khouider and Majda*, 2006a; *Waite and Khouider*, 2010; *Mapes and Neale*, 2011; *Del Genio et al.*, 2012].

The present study emphasizes the fact that the mechanisms for the initiation and propagation of MISO are similar to that of MJOs [*Ajayamohan et al.*, 2013]. The seasonal mean monsoon depends on the relative strengths of the slowly varying boundary forcings and the internal forcings like MISO. Hence, understanding the primary mechanisms of MISO initiation and propagation is key. Several mechanisms have been proposed in the past including wind induces surface evaporation, ocean-atmospheric coupling and boundary layer convergence [*Wang*, 2012]. Here, using a simple model we highlight the fact that capturing the chaotic organization of the tropical convection is the primary mechanism for simulating realistic MISOs.

The paper is organized as follows. The diagnostics used in analyzing the results are described in Section 2. Discussion of the results and conclusions are outlined in Section 3. Videos showing the detailed evolution and propagation of the MJO and MISO are provided in the supplementary material.

2. MISO Diagnostics

The details of the Multicloud_HOMME Model (MHM) configuration and set up are found in *Khouider et al.* [2011] and outlined in the auxiliary material for completeness. All simulations below involve a coarse grid of roughly 167 Kms at the equator. To replicate the northward migration of the TCZ, we conduct three different simulations with a fixed but non-homogeneous SST's mimicking the IO/WP warm pool centered at three northern latitudes, 5°N (WP_5N), 10°N (WP_10N), and 15°N (WP_15N), respectively. The aquaplanet model runs were carried out for 2000 days for each case and the last 1000 days are analyzed to estimate the mean and intraseasonal characteristics of the monsoonal winds and precipitation. The tropical mask at 30°S-30°N, seems to limit the meridional extent of the mean monsoon trough and thereby arresting the poleward propagating signal of the MISO anomalies when the WP is located at 15°N. Hence, for WP_15N experiment, the tropical mask is expanded to 40°S-40°N.

The mean low-level (850hPa) winds and vorticity for the three cases together with the associated regional Hadley cell are plotted in Fig. 1. The low-level mean circulation depicts the turning of the equatorial easterlies to westerlies resulting in a strong cross-equatorial low-level jet and south-westerlies similar to the mean monsoonal flow over the south-Asian continent during the boreal summer [*Goswami and Ajayamohan*, 2001]. The upper-level (200hPa, not shown) mean winds are easterlies overall resulting in a vertical structure that transitions from barotropic along the equator to strongly baroclinic over the warm pool. In observations, the mean monsoon precipitation shows two zones of precipitation maxima, one over the continent and Bay-of-Bengal and another over the warm waters of the Indian Ocean (IO). Another feature of the mean monsoon circulation is that the ascending branch of the regional Hadley cell is located over the monsoon trough region with the descending branch over the IO [*Goswami and Ajayamohan*, 2001]. Our first test is to check whether the mean monsoon circulation is simulated realistically when the WP is moved northward. The two experiments WP_10N and WP_15N simulate well the mean monsoon circulation with the turning of winds from easterlies to westerlies over the eastern edge of the WP although the simulated winds are strong when the WP is located at 15°N (Fig. 1c,e). This results in a cyclonic vorticity pattern over the lower latitudes and an anticyclonic vorticity pattern above it. When the WP is over 5°N, the zonal extend of these patterns are small, although turning of easterlies to westerlies are simulated (Fig. 1a). A zonally narrow regional Hadley cell prevails over the location of the heat source when the WP is at 5°N (Fig. 1b). When the WP is moved poleward, the regional Hadley cell expands in the meridional direction (Fig. 1d,f). Note that the ascending branch of the Hadley cell is at 12°N, even when the WP is moved to 15°N, due to the effect of planetary rotation on diminishing organized convection [*Majda et al.*, 2014]. In summary, this aquaplanet model with the simplified three cloud parameterization scheme simulates the overall mean features of the monsoon circulation realistically. The fine scale features of the mean monsoon circulation like the change of westerlies to easterlies over the Bay-of-Bengal is not simulated by this model probably due to the absence of land.

MISOs propagate northward and eastward simultaneously [*Lawrence and Webster*, 2002; *Wang et al.*, 2005; *Ajayamohan and Goswami*, 2007]. *Lawrence and Webster* [2002] notes that ≈80% of the northward propagating intraseasonal oscillations also exhibit eastward propagating character. When the WP is at 5°N, the MHM mimics the typical character of summer MJOs with a strong eastward propagation (Fig. 2d) and a weak northward propagation (Fig. 4a). A succession of MJO-like events are clearly seen in both zonal winds and precipitation. They are formed over the warm pool and propagate slowly eastward at roughly $5ms^{-1}$. Often as in nature *Lawrence and Webster* [2002],the precipitation propagates northeastward as the MJO-like wave passes through the eastern side of the warm pool while the strongest winds continue to propagate parallel to the equator. See the video of the MJO in the supplementary material. Before exiting the WP region, these MJO-like signals trigger fast moving streaks of wind disturbances that continue to move eastward but at a much faster speed of roughly 25ms^{-1}. These circumnavigating dry Kelvin waves act as a precursor for the successive MJOs [*Ajayamohan et al.*, 2013]. When the WP is moved further north to 10°N, both the eastward and northward propagating character of precipitation and low-level wind anomalies becomes evident (Fig. 2e,Fig. 4b), as in observations. When compared to the WP_5N case, WP_10N case exhibits weaker eastward propagation and stronger northward propagation. The MHM simulation exhibits westward propagating MISOs when the WP is moved further north to 15°N (Fig. 2f). It may be noted that in the observations, when the monsoon is at the peak phase westward propagating synoptic disturbances become active over the monsoon trough region. The northward propagation of MISO anomalies are also evident (Fig. 4c), however the signal is weak compared to the WP_10N case (Fig. 4b).

The characteristics of the simulated MISOs are further illustrated in Fig. 3, where snapshots of the filtered precipitation and low-level winds are plotted for a typical phase of the oscillation. The dominant eastward propagating character of summer MJOs is clearly visible when the WP is at 5°N (Fig. 3a-d). Similarly northward and eastward propagation is evident when the WP is at 10°N (Fig. 3e-h). The boreal summer monsoon can be also viewed as a see-saw representing the rocking oscillation of the TCZ, between its two preferred locations [*Sikka and Gadgil*, 1980; *Gadgil*, 2003; *Goswami and Ajayamohan*, 2001; *Goswami*, 2012]. WP_10N simulations realistically simulates this rocking oscillation of the TCZ. When convection becomes active over the equatorial region (Fig. 3e), suppressed convection prevails over the WP region and vice-versa. The eastward and northward propagation of MISOs, its amplification over the WP, subsequent weakening and triggering of the next MISO over the entire time period of MHM simulations is further illustrated in the movies provided in the auxiliary material.

In addition to the diagnostics presented here, a combined empirical orthogonal function (CEOF) analysis is carried out to identify the dominant mode of the MHM simulations. Fig. 4d shows the first CEOF of the low-level winds when the WP is at 10°N over the WP. The spatial structure has a lot of similarity to the mean monsoon circulation (Fig. 1c) illustrating the common mode of similarity between MISOs and the mean monsoon circulation [*Goswami and Ajayamohan*, 2001]. Moreover, the CEOF1 pattern illustrates well the see-saw oscillation of the TCZ between the equatorial region and the location of the WP. The power spectra of PC1 of the leading EOF shows two dominant peaks, one around 6 days and another around 48 days, illustrating the synoptic and intraseasonal character of the MISOs. In summary, MISO-like oscillations simulated by the MHM has many other, if not all, the, primary features of the MISO as observed in nature.

3. Summary and Discussion

Here, we showed that by coupling a simple multicloud parameterization scheme to the dry dynamic core of an aquaplanet GCM and prescribing a WP, poleward propagating MISOs are realistically simulated. Several theories for the initiation, propagation and scale selection of the MISO have been proposed in the past [*Wang*, 2012]. The multicloud model parameterization [e.g. *Khouider and Majda*, 2006a] is designed based on the observed cloud structure and hence the none of the following mechanisms are present in the MHM simulations. The model is devoid of Wind Induced Surface Heat Exchange

(WISHE), wave-CISK (Convective Instability of the Second Kind), boundary layer friction (FCI), cloud radiation forcing (CRF), ocean/sea-surface dynamics. Nevertheless, the MHM produces realistic MISO-like events with dynamical and physical features that resemble observations. This underlines the role of multicloud mechanism in the initiation and propagation of MISOs.

Based on observational and reanalysis datasets, a few studies have identified that shallow clouds in the lower troposphere lead deep convection and play a critical role in moving the deep convection northward [*Jiang et al.*, 2004, 2010; *Abhik et al.*, 2013]. This means that lower level moistening and the associated mid-tropospheric heating are key processes which determine the northward propagation of MISOs [*Abhik et al.*, 2013]. By design, the multicloud model captures this phenomenology. The intraseasonal oscillations like MJO/MISO and embedded disturbances involve the multicloud structure: a deep convective core preceded by shallow convection or congestus clouds and trailed by upper-tropospheric stratus clouds [*Johnson et al.*, 1999; *Mapes et al.*, 2006; *Jiang et al.*, 2010; *Abhik et al.*, 2013]. When properly coupled to moisture, a two vertical mode model, the first and second baroclinic modes, can generate coherent instability sufficient to initiate intraseasonal oscillations [*Khouider and Majda*, 2006a, b]. The convection takes the form of an envelope of mesoscale and synoptic scale systems involving multiple cloud types which are embedded in and coupled with large-scale monsoonal circulation [*Johnson et al.*, 1999; *Nakazawa*, 1988].

The fact that the dynamical coupling of congestus, deep, and stratiform heating profiles based on the first two baroclinic modes of vertical structure is systematically represented in the multicloud model might be the reason for the successful simulation of MISOs in the MHM simulations. In this model, parameterized convection is not confined into a single grid column and single time step but distributed over the length and time scales of the mesoscale convective systems and synoptic scale systems embedded in the MISOs, unlike traditional cumulus parameterizations.

References

Abhik, S., M. Halder, P. Mukhopadhyay, X. Jiang, and B. Goswami (2013), A possible new mechanism for northward propagation of boreal summer intraseasonal oscillations based on trmm and merra reanalysis, *Clim. Dynam.*, *40*(7-8), 1611–1624, doi:10.1007/s00382-012-1425-x.

Ajayamohan, R. S., and B. N. Goswami (2007), Dependence of simulation of boreal summer tropical intraseasonal oscillations on the simulation of seasonal mean, *J. Atmos. Sci.*, *64*, 460–478, doi:10.1175/JAS3844.1.

Ajayamohan, R. S., B. Khouider, and A. J. Majda (2013), Realistic initiation and dynamics of the Madden-Julian Oscillation in a coarse resolution GCM, *Geophys. Res. Lett.*, *40*, doi:10.1002/2013GL058187.

Bhat, G. S., et al. (2001), BOBMEX: The Bay Of Bengal Monsoon Experiment, *Bull. Amer. Meteorol. Soc.*, *82*(10), 2217–2243, doi:10.1175/1520-0477(2001)082⟨2217:BTBOBM⟩2.3.CO;2.

Crueger, T., B. Stevens, and R. Brokopf (2013), The Madden-Julian Oscillation in ECHAM6 and the introduction of an objective MJO metric, *J. Climate*, *26*, 3241–3256, doi:10.1175/JCLI-D-12-00413.1.

Del Genio, A. D., Y. Chen, D. Kim, and M.-S. Yao (2012), The MJO transition from shallow to deep convection in CLOUDSAT/CALIPSO data and GISS GCM simulations, *J. Climate*, *25*, 3755–3770, doi:10.1175/JCLI-D-11-00384.1.

Gadgil, S. (2003), The Indian monsoon and it's variability, *Annu. Rev. Earth Planet. Sci.*, *31*, 429–467.

Goswami, B. N. (2012), South Asian monsoon, in *Intraseasonal Variability in the Atmosphere-Ocean Climate System*, edited by W. K. M. Lau and D. E. Waliser, chap. 2, pp. 21–72, Springer, Heidelberg, Germany, doi:10.1007/978-3-642-13914-7.

Goswami, B. N., and R. S. Ajayamohan (2001), Intraseasonal oscillations and interannual variability of the Indian summer monsoon, *J. Climate*, *14*, 1180–1198.

Jiang, X., T. Li, and B. Wang (2004), Structures and mechanisms of the northward propagating boreal summer intraseasonal oscillation, *J. Climate*, *17*, 1022–1039.

Jiang, X., D. E. Waliser, J. Li, and C. Woods (2010), Vertical cloud structures of the boreal summer intraseasonal variability based on CloudSat observations and ERA-interim reanalysis, *Clim. Dynam.*, *36*, doi:10.1007/s00382-010-0853-8.

Johnson, R. H., T. M. Rickenbach, S. A. Rutledge, P. E. Ciesielski, and W. H. Schubert (1999), Trimodal characteristics of tropical convection, *J. Climate*, *12*(8), 2397–2418.

Khouider, B., and A. J. Majda (2006a), A simple multicloud parameterization for convectively coupled tropical waves. part i: Linear analysis, *J. Atmos. Sci.*, *63*, 1308–1323.

Khouider, B., and A. J. Majda (2006b), Model multi-cloud parameterizations for convectively coupled tropical waves: Detailed nonlinear wave evolution, *Dynam. Atmos. Oceans*, *42*, 59–80.

Khouider, B., A. St-Cyr, A. J. Majda, and J. Tribbia (2011), The MJO and convectively coupled waves in a coarse resolution GCM with a simple multicloud parameterization, *J. Atmos. Sci.*, *68*, 240–264, doi:101.1175/2010JAS3443.1.

Kim, D., et al. (2009), Application of MJO simulation diagnostics to climate models, *J. Climate*, *22*(23), 6413–6436, doi:10.1175/2009JCLI3063.1.

Lau, W. K. M., and D. E. Waliser (Eds.) (2012), *Intraseasonal Variability in the Atmosphere-Ocean Climate System*, 613 pp., Springer, Heidelberg, Germany, doi: 10.1007/978-3-642-13914-7.

Lawrence, D. M., and P. J. Webster (2002), The boreal summer intraseasonal oscillation: Relationship between northward and eastward movement of convection, *J. Atmos. Sci.*, *59*, 1593–1606.

Lin, J.-L., et al. (2006), Tropical intraseasonal variability in 14 ipcc ar4 climate models part i: Convective signals., *J. Climate*, *19*, 26652690.

Madden, R. A., and P. R. Julian (1971), Detection of a 40-50 day oscillation in the zonal wind in the tropical Pacific, *J. Atmos. Sci.*, *28*, 702–708.

Majda, A. J., B. Khouider, and Y. Frenkel (2014), Effects of rotation and mid-troposphere moisture on organized convection and convectively coupled waves, *Clim. Dynam.*, p. submitted.

Mapes, B., S. Tulich, J. Lin, and P. Zuidema (2006), The mesoscale convection life cycle: Building block or prototype for large-scale tropical waves?, *Dynam. Atmos. Oceans*, *42*, 3–29, doi:10.1016/dynatmoce.2006.03.003.

Mapes, B. E., and R. B. Neale (2011), Parameterizing convective organization to escape the entrainment dilemma, *J. Adv. Model. Earth Sys.*, *3*, M06,004.

Nakazawa, T. (1988), Tropical super clusters within intraseasonal variations over the western Pacific, *J. Meteorol. Soc. Japan*, *66*(6), 823–839.

Rao, P. S. (2005), ARMEX: The Arabian Sea Monsoon Experiment: An overview, *Mausam*, *56*, 1–6.

Sikka, D. R., and S. Gadgil (1980), On the maximum cloud zone and the itcz over Indian longitude during southwest monsoon, *Mon. Weather Rev.*, *108*, 1840–1853.

Sperber, K. R., H. Annamalai, I. S. Kang, A. Kitoh, A. Moise, A. Turner, B. Wang, and T. Zhou (2013), The Asian summer monsoon: an intercomparison of CMIP5 vs. CMIP3 simulations of the late 20th century, *Clim. Dynam.*, *25*, 2721–2744, doi:10.007/s00382-012-1607-6.

Waite, M. L., and B. Khouider (2010), The deepening of tropical convection by congestus preconditioning, *J. Atmos. Sci.*, *67*, 2601–2615.

Wang, B. (2012), Theory, in *Intraseasonal Variability in the Atmosphere-Ocean Climate System*, edited by W. K. M. Lau and D. E. Waliser, chap. 10, pp. 335–398, Springer, Heidelberg, Germany, doi:10.1007/978-3-642-13914-7.

Wang, B., P. J. Webster, and H. Teng (2005), Antecedents and self-induction of active-break south asian monsoon unraveled by satellites, *Geophys. Res. Lett.*, *32*(4), doi:10.1029/2004GL020996.

Zhang, C. (2005), Madden-Julian Oscillation, *Rev. Geophys.*, *43*, RG2003, doi:10.1029/2004RG000158.

Zhang, C., J. Gottschalck, E. Maloney, M. Moncrieff, F.Vitart, D. Waliser, B. Wang, and M. Wheeler (2013), Cracking the MJO nut, *Geophys. Res. Lett.*, doi:10.1002/grl.50244.

Acknowledgments. Center for Prototype Climate Modelling (CPCM) is fully funded by the Abu Dhabi Government through New York University Abu Dhabi (NYUAD) Research Institute grant. This research was initiated during an extended visit of BK and AM to the CPCM at NYUAD during winter 2014. The computations were carried out on the High Performance Computing resources at NYUAD and early tuning of the code were done at the University of Victoria using the West Grid computing Network. The research of AM is partially supported by Office of Naval Research Grant ONR MURI N00014-12-1-0912. The research of BK is partially funded by Monsoon Mission Project, MoES, Government of India.

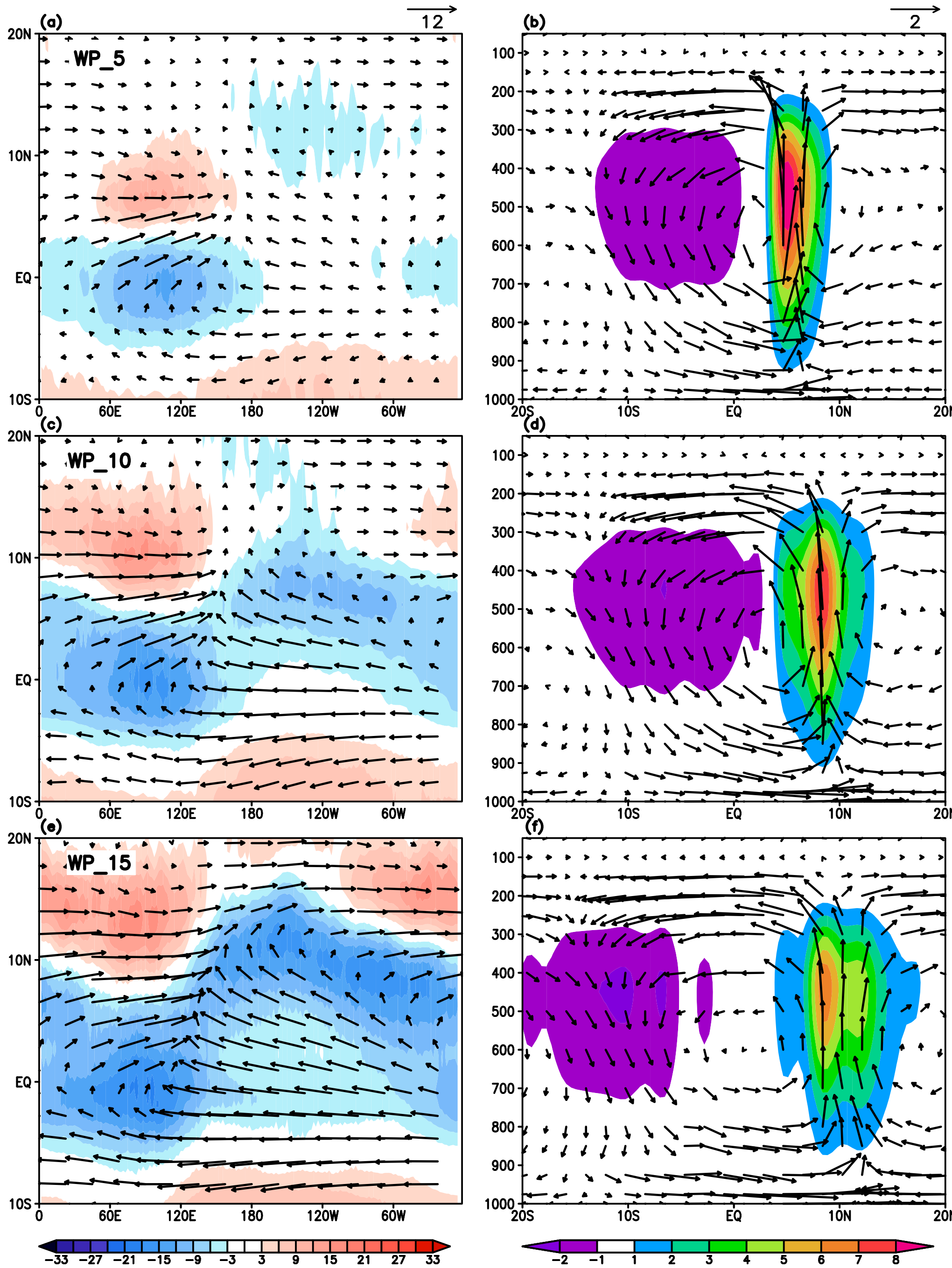

Figure 1. Simulation of the mean monsoon and regional Hadley cell. (a,c,d) Mean 850hPa winds (vectors, ms^{-1}) and relative vorticity (shaded, $x10^{-6}s^{-1}$) for the three sensitivity experiments. (b) Meridional winds and vertical velocity (vector, ms^{-1}) and total heating (QHe;$K.day^{-1}$) averaged over 40°E-120°E.

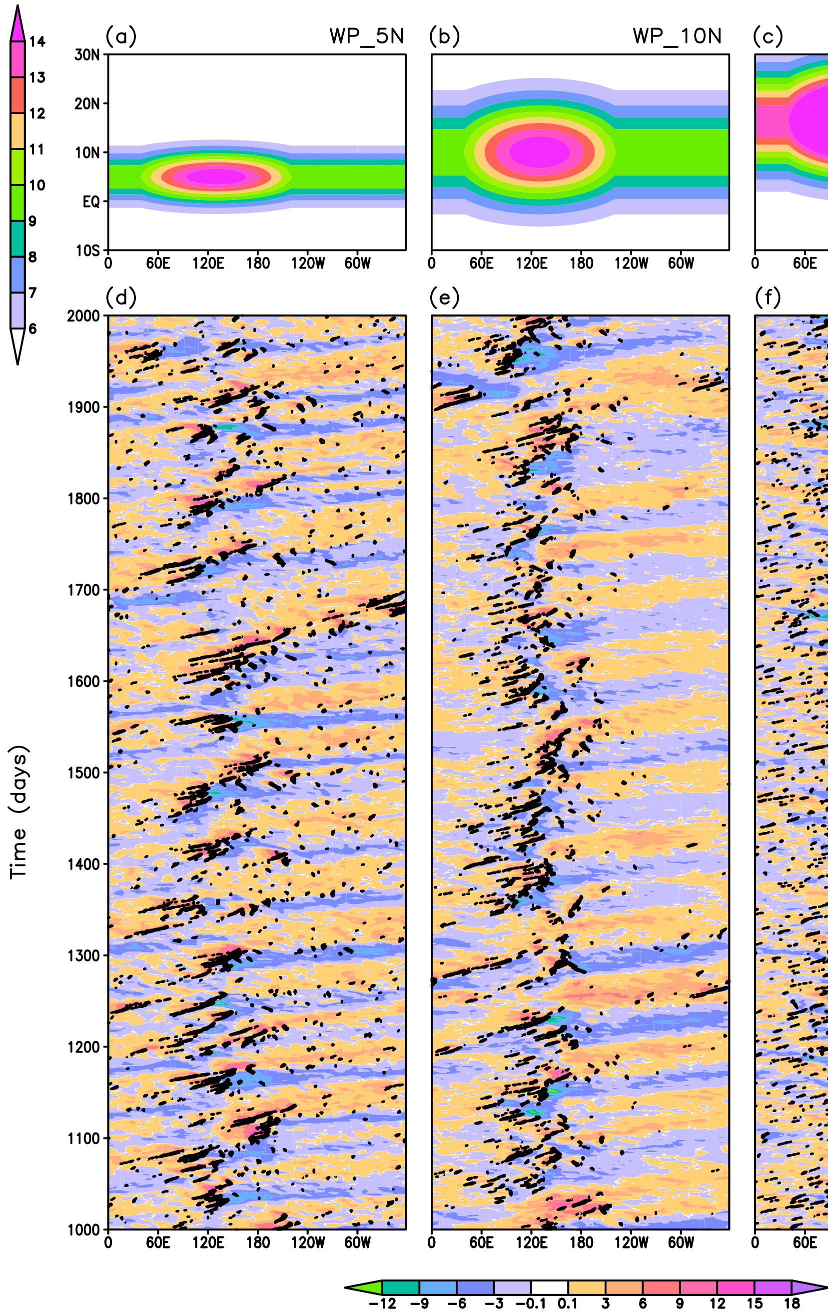

Figure 2. (a,b,c) Structure of the warm pool (°C) used in the simulations. (d,e,f) Hovmöuller plot of low level zonal winds (shaded, ms^{-1}) and precipitation (contour, $K.day^{-1}$) averaged over the domain (0°-15°N) for the various experiments.

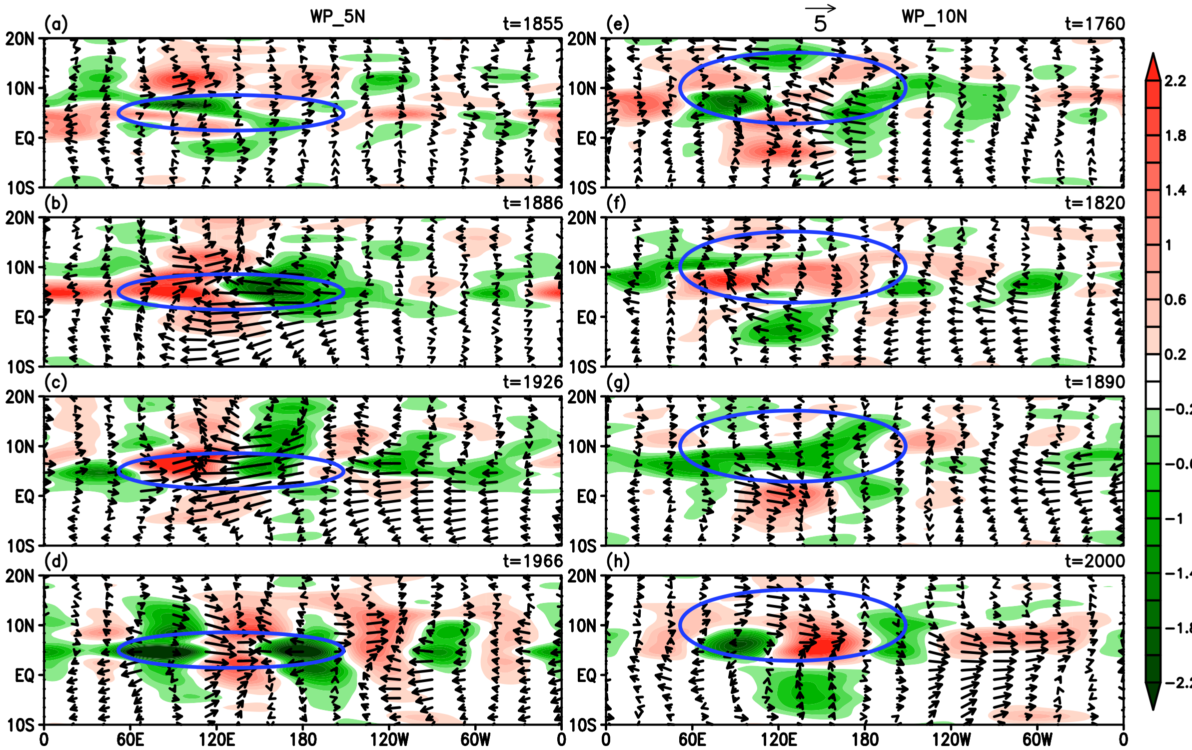

Figure 3. Snapshots of filtered 850hPa winds (vector, ms^{-1}) and precipitation (shaded, $K.day^{-1}$) for a typical oscillation. All the parameters are filtered between wavenumbers ± 4 and time between 20 and 100 days respectively.

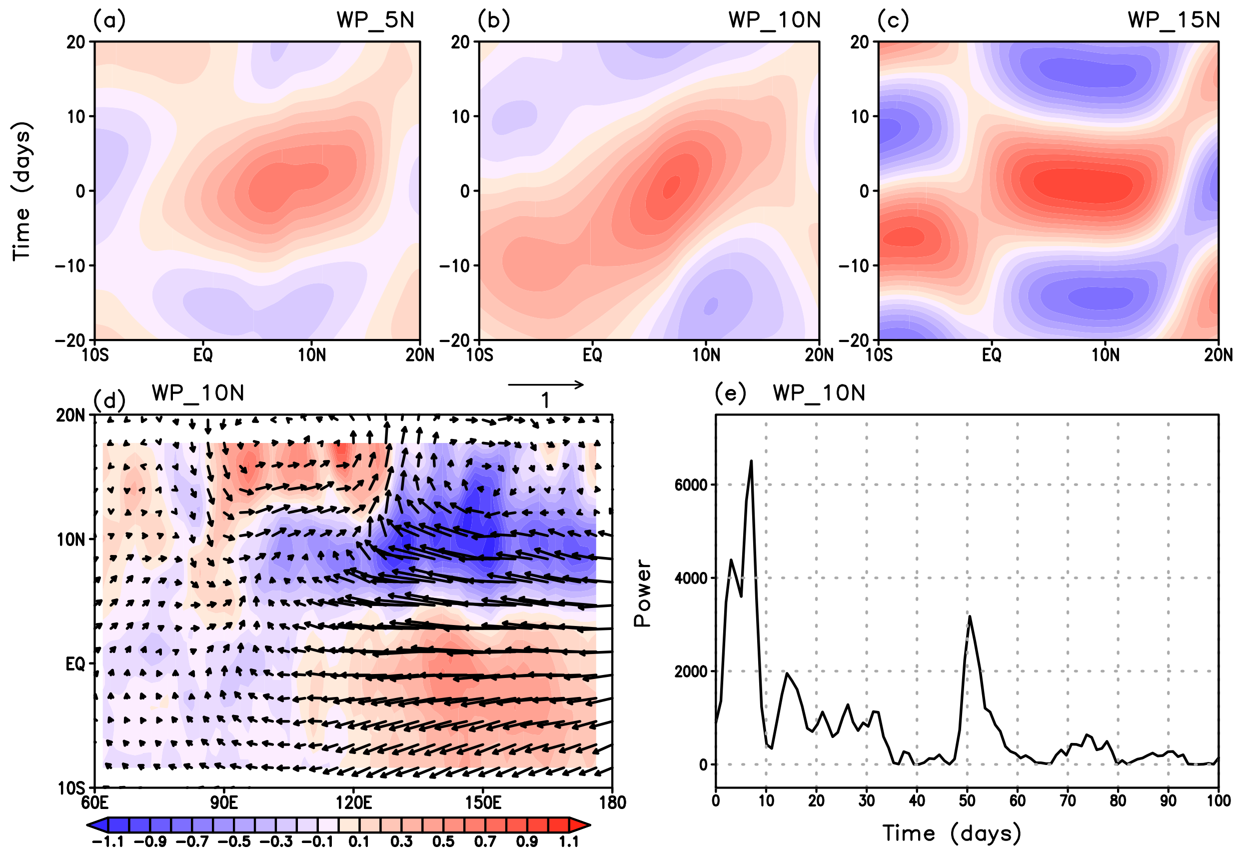

Figure 4. (a-c) Lag-Latitude plots filtered (wave numbers ±4 and 20-100 days) 850hPa zonal winds (ms^{-1}) of MHM simulations for various sensitivity experiments. (d) CEOF1 of 850hpa winds (vectors) and relative vorticity (shaded) anomalies. (e) Power spectra of PC1 of the CEOF.